

An improved dual vector control for a doubly fed induction generator based wind turbine during asymmetrical voltage dips

Youssef Moumani¹, Abdeslam Jabal Laafou¹, Abdessalam Ait Madi¹, Rachid Boutssaid²

¹Advanced Systems Engineering Laboratory, National School of Applied Sciences, Ibn Tofail University, Kenitra, Morocco

²Laboratory of Materials, Signals, Systems and Physical Modeling Faculty of Sciences, Ibn Zohr University, Agadir, Morocco

Article Info

Article history:

Received Nov 30, 2023

Revised Apr 25, 2024

Accepted May 17, 2024

Keywords:

Doubly fed induction generator

Low cost low voltage ride

through

Rotor side converter

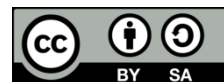
Voltage dip

Wind turbine

ABSTRACT

This paper introduces a robust and enhanced version of dual control approach based on sequence decomposition loops in order to limit transient over-currents and improving the wind turbine's operation during asymmetrical voltage dips faults. Indeed, the doubly fed induction generator (DFIG), employed in wind energy conversion system (WECS) to produce electrical energy from wind, highly susceptible to voltage drops, which can cause transient overcurrents in both the stator and the rotor. Without any protection system, these over-currents might damage the DFIG and its converters. The strategy put forward in this work minimizes the consequences of voltage dips on wind system functioning, such as electromagnetic torque fluctuations and it enables wind turbines to maintain electrical connection with the grid in the occurrence of such disturbances. The carried-out results are promising and showed that the proposed control method can effectively minimise the oscillations in electromagnetic torque, reactive power and DC bus voltage during the asymmetrical voltage dip. This analysis also demonstrated its ability to limit the transient over-currents of the DFIG.

This is an open access article under the [CC BY-SA](#) license.



Corresponding Author:

Youssef Moumani

Advanced Systems Engineering Laboratory, National School of Applied Sciences, Ibn Tofail University

B.P 242, Kenitra, Morocco

Email: youssef.moumani@uit.ac.ma

1. INTRODUCTION

The strong focus on renewable energy sources, in particular wind power, is leading to an increase in installed wind capacity in electricity grids [1]. Due to this high penetration of wind power, to produce green electricity, the grid faces challenges to ensure stability [2]. Consequently, grid codes allow wind systems to participate more actively in maintaining the operability and power quality of the electricity generated and distributed [3]. The doubly fed induction generator (DFIG) based wind power systems have been widely used thanks to their several benefits. The most adopted topology of this type of WECS is illustrated in Figure 1.

However, because the DFIG's stator is directly connected to the grid, when there is a voltage dip, the voltage at the DFIG's terminals rises. and a significant amount of current flows through the stator and rotor windings [3]-[5]. This affects the normal operation of wind turbine (WT) and can lead to the destruction of the DFIG and its converters [6]. WTs were previously permitted to disconnect from the power grid in order to protect themselves from these faults, but this was not beneficial to the producer or the grid operator since disconnecting a wind farm with hundreds of megawatts of power could cause disruptions to the grid and increase the amount of time it took to restore nominal voltage. This is why network operators were constrained to update the standards and requirements of the network codes. Today WTs are no longer

allowed to disconnect during voltage dips and must participate in voltage restoration by injecting reactive power [7]. WT's should behave as much like conventional power stations as possible.

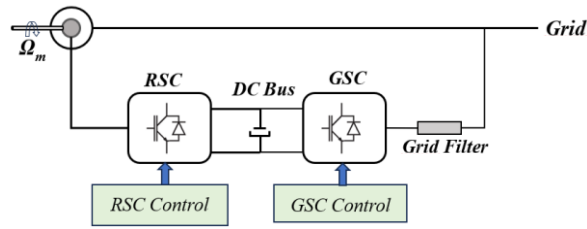


Figure 1. DFIG based WECS topology

In order to keep WT protected and efficient while connected to the grid in case of the voltage sags, several protection approaches have been proposed and documented. These approaches can be classified into two broad categories [8]-[10]: the first category focus on improving control schemes (software solution), while the second category is based on hardware solutions (adding auxiliary equipment) [11]-[16]. In this research paper we will be focusing on the first category that represents a low cost low voltage ride through (LVRT) solution to deal with transients during grid disturbances.

In the literature, several studies were conducted to deal with this issue. Wang *et al.* [17] and Lopez *et al.* [18] are among the main contributors in this research area. These two studies have given thorough backdrop about the dynamic behaviour of DFIG_WT under most typical voltage dips. Thus, other contributors have exploited their results to build a modified control strategies as Mensou *et al.* did in [19]. In this recent interesting study, they developed a direct power control method (DPC), but it's limited only to the operation of DFIG wind turbine under symmetrical voltage dips. Moreover, in this context, another study is performed by Kerrouche *et al.* [20] in which they proposed a dual sequence decomposition. Technique and Lyapunov based control which is very performant as it minimises transient oscillations compared to conventional vector control. However, in this study the performance of the controller proposed is tested during asymmetrical voltage dips type A (phase-ground fault). In order to extend the research work in this direction we propose a modified and improved control approach based dual sequence decomposition of grid voltage and current to control the DFIG-WT. In addition, the performance of this method will be evaluated under unbalanced voltage dips type C (phase-phase_ground fault). Which is one of the most typical power grid disturbances.

This paper is organised as follows: at first the normal operation mode of the DFIG is presented in section 2. Next, its dynamic behaviour under voltage dips is studied in section 3. After that, the control strategy proposed is designed and applied to the WECS in section 4. In order to evaluate the effectiveness and robustness of this controller simulation results obtained are analysed and discussed in section 5. Finally, conclusions and future perspectives are summarised in section 6.

2. NORMAL OPERATION MODE OF DFIG

The equivalent circuit of DFIG is given in Figure 2. As mentioned by [19]-[23] the park model of DFIG is described using (1):

$$\begin{cases} \vec{v}_s = R_s \vec{i}_s + \frac{d\vec{\psi}_s}{dt} \\ \vec{v}_r = R_r \vec{i}_r + \frac{d\vec{\psi}_r}{dt} - j\omega_m \vec{\psi}_r \\ \vec{\psi}_s = L_s \vec{i}_s + L_m \vec{i}_r \\ \vec{\psi}_r = L_r \vec{i}_r + L_m \vec{i}_s \end{cases} \quad (1)$$

With all rotor variables are referred to the stator and ω_m is the electrical speed of the rotor. Since the rotor flux is calculated by (2):

$$\vec{\psi}_r = \frac{L_m}{L_s} \vec{\psi}_s - \sigma L_r \vec{i}_r \quad (2)$$

The expression of the rotor voltage is given by (3):

$$\vec{v}_r = \vec{v}_{r0} + \vec{v}_{r1} \quad (3)$$

Where \vec{v}_{r0} corresponds to the rotor voltage when the rotor windings are open-circuited and \vec{v}_{r1} is a term that is added to the expression of \vec{v}_r when the rotor is connected to rotor side converter (RSC) ($\vec{i}_r \neq 0$) [4]:

$$\begin{cases} \vec{v}_{r0} = \frac{L_m}{L_s} \left(\frac{d}{dt} - j\omega_m \right) \vec{\Psi}_s \\ \vec{v}_{r1} = \left(R_r - \sigma L_r \left(\frac{d}{dt} - j\omega_m \right) \right) \vec{i}_r \end{cases} \quad (4)$$

In normal operating conditions the stator resistance R_s is negligible especially for high power generators which is the case of this proposed study, thus the expression of rotor voltage caused by the forced rotor flux is calculated by (5):

$$\vec{v}_{r0} = g \frac{L_m}{L_s} \widehat{V}_s \quad (5)$$

Where g is the slip of the generator and \widehat{V}_s is the amplitude of stator voltage.

The resistance R_r and transient inductance σL_r of the rotor are often very low. Depending on the speed variation range, rotor currents have a relatively small frequency ($\omega_r \leq 15$ Hz). Therefore, the value of v_r , given by (6), won't differ too much from v_{r0} .

$$\vec{v}_r = \vec{v}_{r0} \quad (6)$$

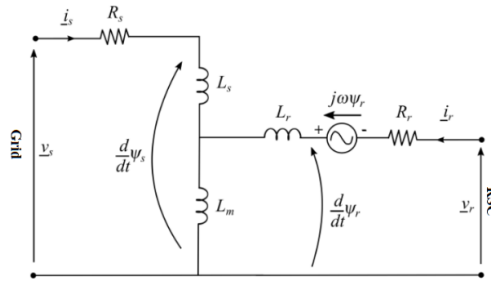


Figure 2. Equivalent circuit of DFIG

3. DFIG BEHAVIOUR DURING VOLTAGE DIP

Often, faults causing voltage dips do not always affect the three phases in the same way. In fact, more than 90% of power system faults result in asymmetrical voltage dips [17]. The effects of asymmetrical faults on the generator are much more significant. Consequently, it is very judicious to study the behaviour of the generator in the case of asymmetrical voltage dips.

According to the theory of symmetrical components developed by Fortescue. The positive, negative, and homopolar components of an asymmetrical three-phase system can be added together. The space vector of the stator voltage, given by (7), can therefore be broken down into three vectors, one for each component.

$$\vec{v}_s = \vec{V}_1 e^{j\omega_s t} + \vec{V}_2 e^{-j\omega_s t} + \vec{V}_0 \quad (7)$$

The Figure 3 shows an example of a 50% asymmetrical voltage dip. The fault affecting the system is a voltage dip type C (phase-phase-ground), where the voltages of the phases “b” “c” and drops by 50% of its nominal value. Figure 3(a) illustrates the time evolution of the voltage before and after the voltage dip, while Figure 3(b) shows the signature of this dip.

Assuming identical impedances, the positive sequence generates a flux that rotates at synchronism speed, while the negative sequence generates a flux that rotates at the same speed but in the opposite direction. The zero sequence produces no flux. In steady state, the forced flux consists of two terms that correspond to the stator voltage's positive and negative components. If the stator resistance (R_s) is ignored, these fluxes, noted by ψ_{s1} and ψ_{s2} , can be expressed by (8) [3]:

$$\begin{cases} \vec{\psi}_{s1} = \frac{\vec{V}_1}{j\omega_s} e^{j\omega_s t} \\ \vec{\psi}_{s2} = -\frac{\vec{V}_2}{j\omega_s} e^{-j\omega_s t} \end{cases} \quad (8)$$

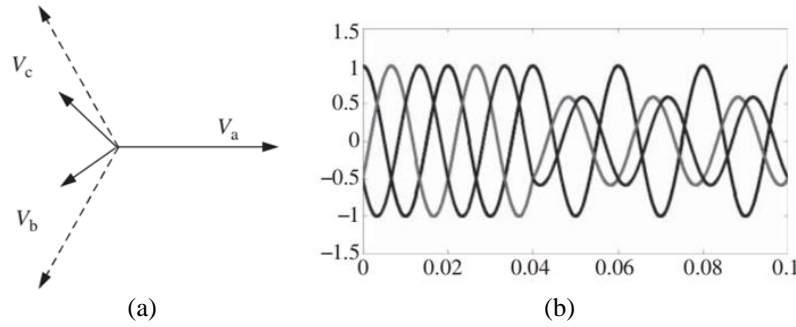


Figure 3. 50% asymmetrical voltage type C (phase-phase fault); (a) vector representation and (b) abc voltages

The natural flux appears at the first moments. The total stator flux is therefore expressed by (9):

$$\vec{\psi}_s = \frac{\vec{V}_1}{j\omega_s} e^{j\omega_s t} + -\frac{\vec{V}_2}{j\omega_s} e^{-j\omega_s t} + \vec{\psi}_{n0} e^{-\frac{t}{\tau_s}} \quad (9)$$

The total rotor voltage induced in an open circuit is then given by (10):

$$\vec{\psi}_s = \frac{\vec{V}_1}{j\omega_s} e^{j\omega_s t} + -\frac{\vec{V}_2}{j\omega_s} e^{-j\omega_s t} + \vec{\psi}_{n0} e^{-\frac{t}{\tau_s}} \quad (10)$$

By substituting (8) into (4), In the rotor reference frame, the two rotor voltages generated by the positive and negative sequences can be stated with (11):

$$\begin{cases} \vec{v}_{r1}^{(r)} = \hat{V}_1 \frac{L_m}{L_s} g e^{jg\omega_s t} \\ \vec{v}_{r2}^{(r)} = \hat{V}_2 \frac{L_m}{L_s} (2 - g) e^{-j(2-g)\omega_s t} \end{cases} \quad (11)$$

Since the slip g is generally low, the amplitude of $v_{r1}^{(r)}$ will be low and that of $v_{r2}^{(r)}$ will be relatively high. The rotor voltage induced by natural flux is expressed in the rotor reference by (12) [24]:

$$\vec{v}_{rn}^{(r)} = -\frac{L_m}{L_s} \left(\frac{1}{\tau_s} + j\omega_m \right) \vec{\psi}_{n0} e^{-\frac{t}{\tau_s}} e^{-j\omega_m t} \quad (12)$$

With the term $\frac{1}{\tau_s}$ negligible the previous expression becomes:

$$\vec{v}_{rn}^{(r)} = -j\omega_m \frac{L_m}{L_s} \vec{\psi}_{n0} e^{-\frac{t}{\tau_s}} e^{-j\omega_m t} \quad (13)$$

The initial value of natural flux ($\vec{\psi}_{n0}$) at t_0 is illustrated by (14):

$$\begin{cases} \vec{\psi}_s(t_0^-) = \vec{\psi}_s(t_0^+) \\ \vec{\psi}_s(t_0^+) = \vec{\psi}_{n0} = \vec{\psi}_s(t_0^-) - [\vec{\psi}_{s1}(t_0^+) + \vec{\psi}_{s2}(t_0^+)] \end{cases} \quad (14)$$

The second in (14) shows that the amplitude of $\vec{\psi}_{n0}$ depends on the instant at which the fault starts, in other words, it depends on the phase angle between the positive and negative sequence of the flux at the instant of the trough t_0 . This phase angle changes with time due to the opposing rotational directions of the two flux terms. Consequently, the result of the previous equation depends on the moment of start of the voltage dip.

4. APPLICATION OF SEQUENCE DECOMPOSITION AND DESIGN OF THE CONTROLLER

In this section, a positive and negative sequence decomposition (PNSD) method based on a second order generalised integrator (SOGI) three phase PLL is proposed, in order to: i) extract the components of positive and negative sequences from the three-phase grid voltage; ii) eliminate the second-order harmonics

(including the $2\omega_s$ frequency) due to the negative sequence using a notch filter; iii) ensure independent control of the positive and negative sequences of currents; and iv) improve the system's operating performance. Figure 4 displays the grid voltage's space vector in the synchronous reference frames for both positive and negative sequences.

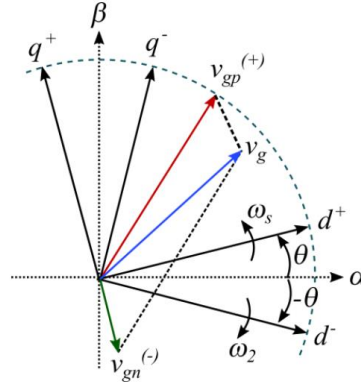


Figure 4. Space vector of the grid voltage in synchronous markers dq(+) and dq(-)

The stator and rotor voltages, currents and fluxes of the DFIG are given by (15) [25], [26]:

$$\begin{cases} v_{sdq}^{(+)} = v_{sdqp}^{(+)} + v_{sdqn}^{(-)} e^{-2j\omega_s t} \\ i_{sdq}^{(+)} = i_{sdqp}^{(+)} + i_{sdqn}^{(-)} e^{-2j\omega_s t} \\ \psi_{sdq}^{(+)} = \psi_{sdqp}^{(+)} + \psi_{sdqn}^{(-)} e^{-2j\omega_s t} \\ v_{rdq}^{(+)} = v_{rdqp}^{(+)} + v_{rdqn}^{(-)} e^{-2j\omega_s t} \\ i_{rdq}^{(+)} = i_{rdqp}^{(+)} + i_{rdqn}^{(-)} e^{-2j\omega_s t} \\ \psi_{rdq}^{(+)} = \psi_{rdqp}^{(+)} + \psi_{rdqn}^{(-)} e^{-2j\omega_s t} \end{cases} \quad (15)$$

The expression for the stator's active and reactive powers is (16):

$$\begin{cases} P_s = \frac{3}{2} \Re \{ v_{sdq}^{(+)} i_{sdq}^{(+)*} \} \\ Q_s = \frac{3}{2} \Im \{ v_{sdq}^{(+)} i_{sdq}^{(+)*} \} \end{cases} \quad (16)$$

Therefore, P_s and Q_s are calculated by (17):

$$\begin{cases} P_s = P_{s0} + P_{sin2} \sin(2\omega_s t) + P_{cos2} \cos(2\omega_s t) \\ Q_s = Q_{s0} + Q_{sin2} \sin(2\omega_s t) + Q_{cos2} \cos(2\omega_s t) \end{cases} \quad (17)$$

With

$$\begin{bmatrix} P_{s0} \\ Q_{s0} \end{bmatrix} = \frac{2}{3} \begin{bmatrix} v_{sdp} & v_{sqp} & v_{sdn} & v_{sqn} \\ v_{sqp} & -v_{sdp} & v_{sqn} & -v_{sdn} \end{bmatrix} \begin{bmatrix} i_{sdp} \\ i_{sqp} \\ i_{sdn} \\ i_{sqn} \end{bmatrix} \quad (18)$$

The electromagnetic torque of the generator is written by (19):

$$T_{em} = \frac{3}{2} p \frac{L_m}{L_s} \Im \{ \psi_{sdq}^{(+)} i_{rdq}^{(+)*} \} \quad (19)$$

The development of (19) leads to the following result:

$$T_{em} = T_{em0} + T_{em\sin2} \sin(2\omega_s t) + T_{em\cos2} \cos(2\omega_s t) \quad (20)$$

With

$$T_{em0} = \frac{3}{2} p \frac{L_m}{L_s} \begin{bmatrix} -v_{sdp} & -v_{sqp} & v_{sdn} & v_{sqn} \end{bmatrix} \begin{bmatrix} i_{rdp} \\ i_{rqp} \\ i_{rdn} \\ i_{rqn} \end{bmatrix} \quad (21)$$

To overcome the undesirable effect of the negative sequence due to the asymmetrical voltage dip, it is desirable to reduce the oscillations of the electrical quantities concerned. To do this, the rotor current references could simply be set to zero for negative sequence and calculated for positive sequence. The control law becomes as illustrated by (22):

$$\begin{bmatrix} i_{rdp}^* \\ i_{rqp}^* \\ i_{rdn}^* \\ i_{rqn}^* \end{bmatrix} = A \begin{bmatrix} v_{sdp} & v_{sqp} \\ v_{sqp} & -v_{sdp} \\ 0 & 0 \\ 0 & 0 \end{bmatrix} \begin{bmatrix} P_{s0} \\ Q_{s0} \end{bmatrix} + \frac{1}{\omega_s L_m} \begin{bmatrix} v_{sqp} \\ -v_{sdp} \\ 0 \\ 0 \end{bmatrix} \quad (22)$$

With $A = -\frac{2L_s}{3L_m(v_{sdp}^2 + v_{sqp}^2)}$. The control objectives of the RSC and grid side converter (GSC) converters can be easily achieved during normal DFIG operation. However, during asymmetrical voltage dips, the behaviour of the DFIG changes and these objectives cannot be easily achieved. Therefore, an appropriate control approach must be adopted for both RSC and GSC converters as depicted in Figures 5 to 7.

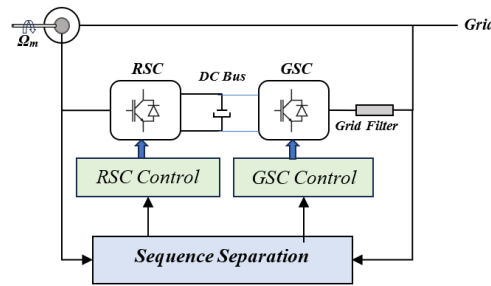


Figure 5. Schematic diagram of the proposed control

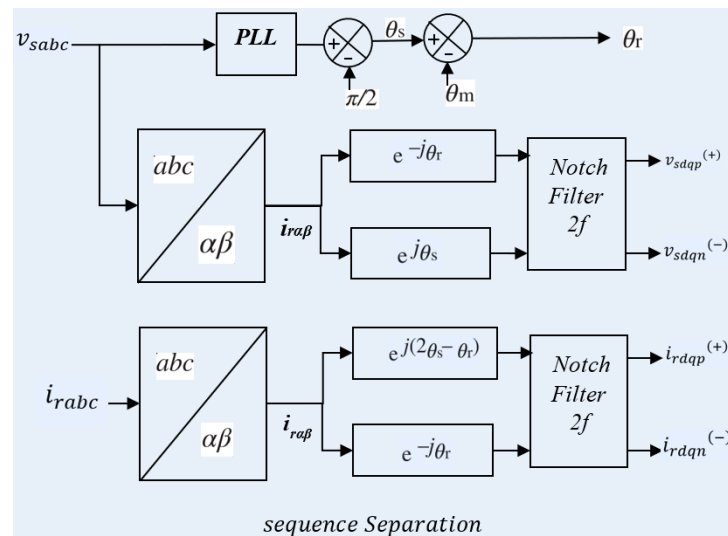


Figure 6. Sequence decomposition loops

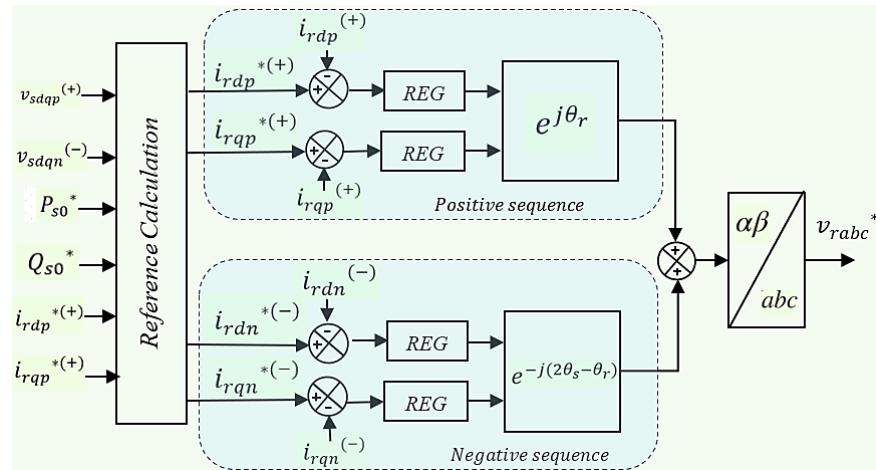


Figure 7. Schematic diagram of the proposed control for RSC converter

5. SIMULATION RESULTS

The suggested control's performance is evaluated using the system's global dynamic model in MATLAB/Simulink-2021a. The voltage dip profile was applied to the system at the time interval 3.5 to 4.5 s as illustrated in Figure 8 that shows the stator voltages. The fault period is brief in comparison to the changes in wind speed, hence the wind speed profile is maintained constant and equal to 8.5 m/s during the fault phase. The system parameters used in the simulations are shown in the Table 1.

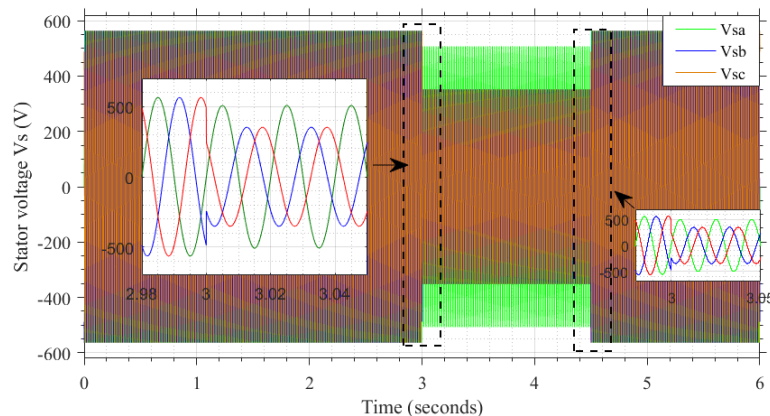
Figure 8. Stator voltages V_s (V)

Table 1. WECS parameters

Parameter name	Symbol	Value	Unit	Parameter name	Symbol	Value	Unit
Rated power	P_n	2	MW	Magnetizing inductance	L_m	2.5	mH
Rated voltage	U_n	690	V	Rated wind speed	v	12	m/s
Nominal frequency	f	50	Hz	Air density	ρ	1,225	kg/m ³
Rated rotor speed	N	1500	rpm	Blade radius	R	42	m
Number of pole pairs	p	2		Gearbox ratio	G	100	
Stator resistance	R_s	2.6	m Ω	DC-link voltage	U_{dc}	1200	V
Rotor resistance	R_r	2.9	m Ω	DC-link capacitor	C	80	mF
Stator leakage inductance	$L_{s\sigma}$	0.087	mH	Filter resistance	R_g	0.02	m Ω
Rotor leakage inductance	$L_{r\sigma}$	0.087	mH	Filter inductance	L_g	0.4	mH

The Figures 9 and 10 show the evolution of rotor current components generated by the controller. In these figures we can obviously see that the currents loops follow their references for both positive and negative components. Consequently they keep control of the torque T_{em} despite some slight fluctuations during transients.

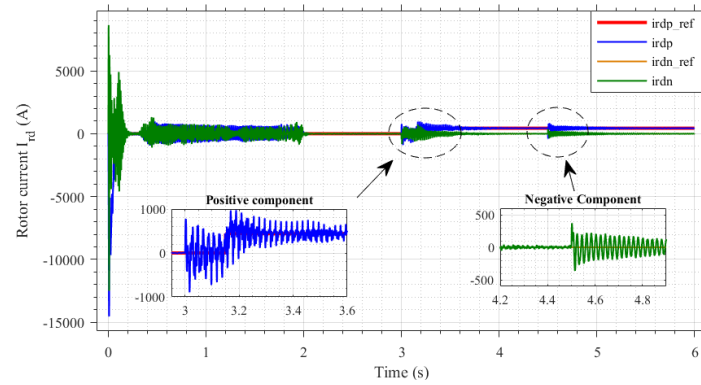
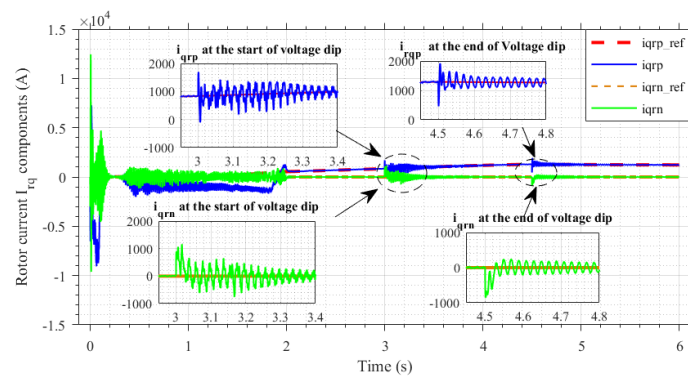
Figure 9. Rotor current (direct component) I_{rd} 

Figure 10. Rotor current (q component) (A)

In Figure 11 one can see the damping of these oscillations of the torque after a very short time. Therefore it will reduce the effects of the unbalanced voltage dip. Since the voltage dip is also seen by the GSC, the same control strategy was applied to keep the DC bus voltage V_{bus} and reactive power. The DC bus voltage response is presented in Figure 12. In this figure, one can see that, despite voltage unbalance disturbance the DC bus voltage is still being able to follow its reference with damped fluctuations at the beginning and at the end of disturbance.

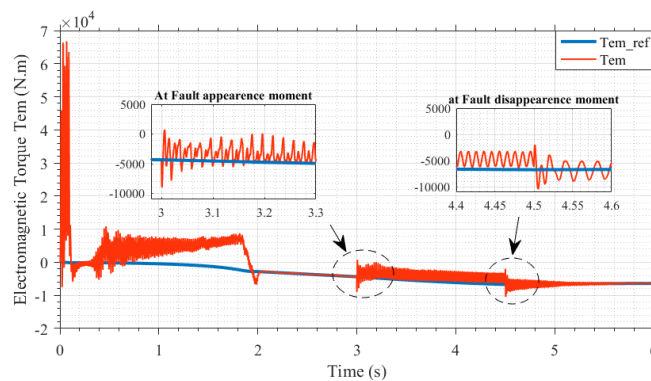
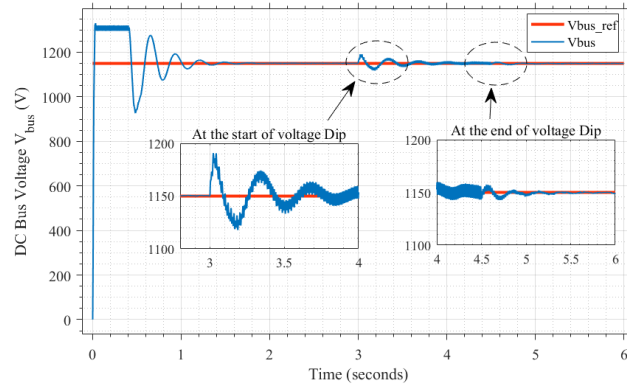
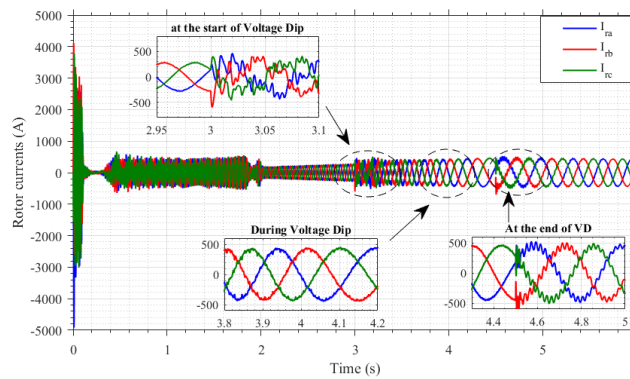
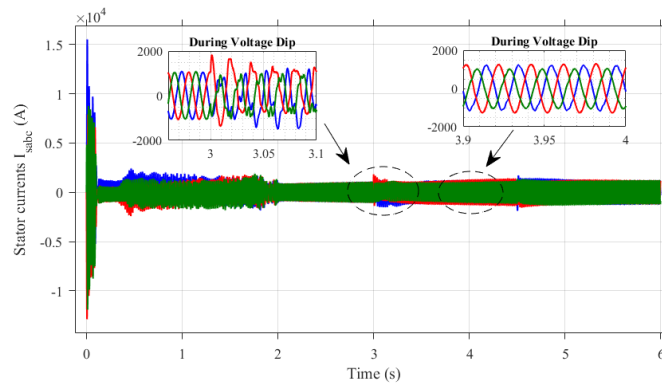


Figure 11. Electromagnetic torque (N.m)

The effectiveness of the control loops for both RSC and GSC converters limit the increase of rotor and stator currents during voltage dip. The currents in the stator and the rotor are shown respectively in Figures 13 and 14 where there are slight oscillations at the start as well as at the disappearance of voltage sag, but due to the fast response of the controller those fluctuations are quickly damped and eliminated.

Figure 12. DC bus voltage V_{bus} (V)Figure 13. Rotor currents I_{abc} (A)Figure 14. Stator currents I_{abc} (A)

6. CONCLUSION

This research presents an investigation of the dynamic behavior of the DFIG_WT under asymmetric voltage dips. Then, a control strategy is proposed as a software solution to improve the transient stability of the DFIG and LVRT capability during and after unbalanced voltage drops event. The analysis of the simulation results showed that the DIGSO-PLL-based PNSD method can effectively minimise the oscillations in electromagnetic torque, reactive power and DC bus voltage during the asymmetrical voltage dip. This analysis also demonstrated its ability to limit the transient over-currents which ensures the protection of the DFIG and power converters. Although this method is more complex to implement and requires more computation time, it does not require any additional devices to be implemented, and it is able

to control fault currents and improve the dynamic behaviour of the DFIG during voltage dips, thus meeting the strict network code requirements for integrating WTs into distribution networks. However, more research efforts should be performed in this direction to design more advanced control algorithms based on non-linear approaches.

ACKNOWLEDGEMENTS

The Advanced Systems Engineering Laboratory at Ibn Tofail University which provided the resources for this research, is warmly acknowledged by the authors. This research is conducted independently and is funded by the researchers themselves and thanks all parties involved.




REFERENCES

- [1] R. Cheikh, H. Belmili, A. Menacer, S. Drid, and L. Chrifi-Alaoui, "Dynamic behavior analysis under a grid fault scenario of a 2 MW double fed induction generator-based wind turbine: comparative study of the reference frame orientation approach," *International Journal of System Assurance Engineering and Management*, vol. 10, no. 4, pp. 632–643, Aug. 2019, doi: 10.1007/s13198-019-00790-0.
- [2] M. Aimene, "System services and management of transient energy interactions in an offshore wind farm (in French: services au système et gestion d'interactions énergétiques transitoires dans un parc éolien offshore)," These de doctorat, Le Havre, 2016.
- [3] M. Fdaili, T. Nasser, A. Essadki, M. Nadour, and I. Kharchouf, "Control strategies for DFIG-based wind turbine systems contributing to LVRT improvement and grid primary frequency adjustment," in *2020 International Conference on Electrical and Information Technologies (ICEIT)*, IEEE, Mar. 2020, pp. 1–6, doi: 10.1109/ICEIT48248.2020.9113195.
- [4] A. J. Laafou, A. A. Madi, Y. Moumani, and A. Addaim, "Improving LVRT for DFIG used in WPCS under voltage dip," in *2023 3rd International Conference on Innovative Research in Applied Science, Engineering and Technology (IRASET)*, IEEE, May 2023, pp. 01–05, doi: 10.1109/IRASET57153.2023.10152878.
- [5] Y. Moumani, A. J. Laafou, and A. Ait Madi, "Modeling and backstepping control of DFIG used in wind energy conversion system," in *2021 7th International Conference on Optimization and Applications (ICOA)*, IEEE, May 2021, pp. 1–6, doi: 10.1109/ICOA51614.2021.9442625.
- [6] P. R. Teja and C. Murali, "Theoretical modeling and simulation of Grid connected DFIG under symmetrical and asymmetrical faults," *International Research Journal of Engineering and Technology (IRJET)*, vol. 3, no. 10, pp. 1078–1085, 2016.
- [7] B. Qin, H. Li, X. Zhou, J. Li, and W. Liu, "Low-voltage ride-through techniques in DFIG-based wind turbines: A review," *Applied Sciences*, vol. 10, no. 6, Mar. 2020, doi: 10.3390/app10062154.
- [8] M. Chakib, T. Nasser, and A. Essadki, "Comparative study of active disturbance rejection control with RST control for variable wind speed turbine based on doubly fed induction generator connected to the grid," *International Journal of Intelligent Engineering and Systems*, vol. 13, no. 1, pp. 248–258, Feb. 2020, doi: 10.22266/ijies2020.0229.23.
- [9] W. Guo et al., "LVRT capability enhancement of DFIG with switch-type fault current limiter," *IEEE Transactions on Industrial Electronics*, vol. 62, no. 1, pp. 332–342, Jan. 2015, doi: 10.1109/TIE.2014.2326997.
- [10] D. Zhu, X. Zou, L. Deng, Q. Huang, S. Zhou, and Y. Kang, "Inductance-emulating control for DFIG-based wind turbine to ride-through grid faults," *IEEE Transactions on Power Electronics*, vol. 32, no. 11, pp. 8514–8525, Nov. 2017, doi: 10.1109/TPEL.2016.2645791.
- [11] I. Kharchouf, A. Essadki, and T. Nasser, "Wind system based on a doubly fed induction generator: Contribution to the study of electrical energy quality and continuity of service in the voltage dips event," *International Journal of Renewable Energy Research*, vol. 7, no. 4, pp. 1892–1900, 2017, doi: 10.20508/ijrer.v7i4.6298.g7232.
- [12] N. Khemiri and A. Khedher, "A comparison of conventional and modified vector control strategies for controlling transient currents and voltage dips in grid-connected wind and photovoltaic hybrid system," *Environmental Progress and Sustainable Energy*, vol. 39, no. 5, Sep. 2020, doi: 10.1002/ep.13415.
- [13] J. Liang, D. Howard, J. Restrepo, and R. Harley, "Feedforward transient compensation control for DFIG wind turbines during both balanced and unbalanced grid disturbances," *Industry Applications, IEEE Transactions on*, vol. 49, no. 3, pp. 1452–1463, May 2013, doi: 10.1109/TIA.2013.2253439.
- [14] X. Yifan, A. Aimin, Z. Yingying, and C. Wei, "Design and implementation of crowbar circuits combined with chopper circuits for LVRT in wind farms," *Journal of Physics: Conference Series*, vol. 1639, no. 1, Oct. 2020, doi: 10.1088/1742-6596/1639/1/012040.
- [15] H. Dong, H. Wu, J. Pan, Y. Chen, and B. Xu, "Research on double-fed induction generator low voltage ride through based on double braking resistors using fuzzy control," *Energies*, vol. 11, no. 5, May 2018, doi: 10.3390/en11051155.
- [16] G. F. Gontijo et al., "Modeling, control, and experimental verification of a DFIG with a series-grid-side converter with voltage sag, unbalance, and distortion compensation capabilities," *IEEE Transactions on Industry Applications*, vol. 56, no. 1, pp. 584–600, Jan. 2020, doi: 10.1109/TIA.2019.2946950.
- [17] A. Wang, S. Shu, and Y. Wang, "Dynamic behavior of DFIG during asymmetrical voltage dips in a coupled simulation," in *2015 18th International Conference on Electrical Machines and Systems (ICEMS)*, IEEE, Oct. 2015, pp. 1051–1058, doi: 10.1109/ICEMS.2015.7385193.
- [18] J. Lopez, P. Sanchis, E. Gubia, A. Ursua, L. Marroyo, and X. Roboam, "Control of doubly fed induction Generator under symmetrical voltage dips," in *2008 IEEE International Symposium on Industrial Electronics*, IEEE, Jun. 2008, pp. 2456–2462, doi: 10.1109/ISIE.2008.4677148.
- [19] S. Mensou, A. Essadki, T. Nasser, and B. B. Idrissi, "A direct power control of a DFIG based-WECS during symmetrical voltage dips," *Protection and Control of Modern Power Systems*, vol. 5, no. 1, Dec. 2020, doi: 10.1186/s41601-019-0148-y.
- [20] K. D. E. Kerrouche, L. Wang, A. Van Den Bossche, A. Draou, A. Mezouar, and L. Boumediene, "Dual robust control of grid-connected DFIGs-based wind-turbine-systems under unbalanced grid voltage conditions," in *Stability Control and Reliable Performance of Wind Turbines*, InTech, 2018, doi: 10.5772/intechopen.75518.
- [21] Y. Moumani, A. J. Laafou, and A. A. Madi, "A comparative study based on proportional integral and backstepping controllers for doubly fed induction generator used in wind energy conversion system," *Archives of Electrical Engineering*, vol. 72, no. 1, pp. 211–228, 2023, doi: 10.24425/aee.2023.143698.




- [22] A. J. Laafou, A. A. Madi, Y. Moumani, and A. Addaim, "Proposed robust ADRC control of a DFIG used in wind power production," *Bulletin of Electrical Engineering and Informatics*, vol. 11, no. 3, pp. 1210–1221, Jun. 2022, doi: 10.11591/eei.v11i3.3539.
- [23] I. Kharchouf, T. Nasser, A. Essadki, and M. Fdaili, "Adaptive fuzzy-PI control of wind energy conversion system based DFIG under voltage dip," in *2020 International Conference on Electrical and Information Technologies (ICEIT)*, IEEE, Mar. 2020, pp. 1–6, doi: 10.1109/ICEIT48248.2020.9113215.
- [24] J. Lopez, E. Gubla, P. Sanchis, X. Roboam, and L. Marroyo, "Wind turbines based on doubly fed induction generator under asymmetrical voltage dips," *IEEE Transactions on Energy Conversion*, vol. 23, no. 1, pp. 321–330, Mar. 2008, doi: 10.1109/TEC.2007.914317.
- [25] W. Yang, H. Zhang, J. Li, A. Zhang, Y. Zhou, and J. Wang, "PIDR sliding mode current control with online inductance estimator for VSC-MVDC system converter stations under unbalanced grid voltage conditions," *Energies*, vol. 11, no. 10, Sep. 2018, doi: 10.3390/en11102599.
- [26] F. Xiao, Z. Zhang, and X. Yin, "Fault current characteristics of the DFIG under asymmetrical fault conditions," *Energies*, vol. 8, no. 10, pp. 10971–10992, Sep. 2015, doi: 10.3390/en81010971.

BIOGRAPHIES OF AUTHORS






Youssef Moumani    received Master degree of Sciences and Technology speciality: automation, signal processing, and industrial computing in 2014, from Faculty of Science and Technology, Hassan I University, Settat, Morocco. He is currently a Ph.D. Student at National School of Applied Sciences, Ibn Tofail University, Kenitra Morocco. His research interests are control strategies of wind power systems. He can be contacted at email: youssef.moumani@uit.ac.ma.






Abdeslam Jabal Laafou    was born in Morocco. He received the Ph.D degree of Electrical Engineering in 2023 from the National School of Applied Sciences, Ibn Tofail University, Kenitra, Morocco. He received the Master degree of Electrical Engineering from the ENSET of Rabat, Mohammed V University, Rabat, Morocco. He is currently a professor of Electrical Engineering. His research interests are control strategies of wind power systems. He can be contacted at email: abdeslam.jaballaafou@uit.ac.ma.



Abdessalam Ait Madi    was born in Morocco. He received the teaching engineering degree in electronics from the ENSET of Mohammedia. He received the Master and Ph.D. degrees from the Faculty of Sciences and Technologies from the Sidi Mohamed Ben Abdellah University of Fez in Morocco. He received the Habilitation degree from the Faculty of Sciences of Ibn Tofail University. He is an Associate Professor at the National School of Applied Sciences of ibn Tofail University in Kenitra, Morocco. He can be contacted at email: abdessalam.aitmadi@uit.ac.ma.



Rachid Boutssaid    received a master's degree in sciences and technologies, specializing in automatic control, signal processing, and industrial computing in 2022 from the Faculty of Science and Technology at Hassan I University, Settat, Morocco. He is currently a Ph.D. student at the Faculty of Science, Ibn Zohr University, Agadir, Morocco. His research interests include the study of performance and control of cyber-physical systems. He can be contacted at email: rachid.boutssaid.56@edu.uiz.ac.ma.